euspen's 24th International Conference & Exhibition, Dublin, IE, June 2024
www.euspen.eu

Non-destructive measurement method for internal surface roughness based on a magnetic tool and machine learning model

Jiong Zhang[1,2*] and Wenwen Tian[1,3,4]

[1]*Department of Mechanical Engineering, Faculty of Engineering, National University of Singapore, 9 Engineering Drive 1, Singapore 117575, Singapore*
[2]*Department of Mechanical Engineering, College of Engineering, City University of Hong Kong, 83 Tat Chee Avenue, Kowloon Tong, Hong Kong SAR, China*
[3]*School of Automation and Electrical Engineering, Lanzhou Jiaotong University, Lanzhou 730070, China*
[4]*School of Mechanical Engineering, Xi'an Jiaotong University, Xi'an 710049, China*

**Corresponding author's Email address: jiongz@u.nus.edu*

Abstract

Surface quality evaluation of internal surfaces is vital while challenging. In this paper, we proposed a novel and non-destructive method for internal surface roughness measurement based on a magnetic tool and a data-driven model named fuzzy broad learning system (FBLS). The magnetic tool is placed on the workpiece's inner surface and dragged by an external magnet. The force between the tool and the workpiece is recorded and used as input for the FBLS. FBLS combines the logical reasoning ability of a fuzzy system with the self-learning ability of a neural network. It is suitable for nonlinear and uncertainty modelling, and the computational efficiency is high. Experiments show that this method is suitable for workpieces with surface roughness (Ra) larger than 1 µm and its average measurement error is only 10.1%, which is adequate for the quality control of most engineering surfaces. This method may be further applied to surface quality evaluation of additively manufactured internal surfaces and complex channels.

Keywords: surface roughness; internal measurement; machine learning; magnetic tool; force signal

1. Introduction

Internal surfaces are widely used in daily life and industries. Representative examples include the tubes in aeroengines, sanitary pipes in the semiconductor industry, conformal cooling channels in precision moulds, manifolds in automobiles, waveguides in communication devices, etc. These internal surfaces are commonly seen as excellent carriers for gas, fluids, or electromagnetic waves [1–3]. The surface quality of these internal surfaces significantly affects their service performance [4,5]. However, there are limited methods to measure the surface finish of these internal surfaces because conventional measurement tools, e.g., a stylus probe or a microscope, cannot access the enclosed space. The most commonly used method is to cut the sample and expose the internal surface so that conventional measurement devices can be employed, which, however, is a typical destructive measurement method. In terms of the tubes with large diameters, the stylus probe can be inserted into them and conduct the profile scanning. Alternatively, an endoscope can also be put inside a tube to measure the profile via white-light interferometry [6]. Some researchers converted the internal measurement to external measurement by a silicone replica [7]. This method is only suitable for some simple tubes and still needs the assistance of a profilometer or a confocal microscope. Regarding more complex components with small openings, X-ray computed tomography (X-ray CT) can be used to obtain their volumetric information via scanning, reconstruction, and data visualization [8,9]. The reconstructed 3D model of the component contains the surface topography information of the internal features. However, the resolution of existing X-ray CT is usually larger than 5 µm and the operating expense is extremely high. Another indirect and non-destructive evaluation method for the surface quality of pipes is by analyzing the acoustic emission (AE) signal which is generated by the flowing liquid [10]. The surface state, either rough or smooth, can be distinguished by comparing the extracted features of the AE signal. Nevertheless, it is impossible to provide an accurate value of the surface roughness. Therefore, a reliable, precise, low-cost, and non-destructive measurement method needs to be developed to tackle the challenge in surface quality evaluation of internal surfaces. In this paper, an indirect measurement system based on a magnetic tool and a fuzzy broad learning model is proposed. A sphere magnet is put inside the workpiece. An external magnet is used to drive the sphere magnet to slide on the surface to be evaluated. A dynamometer is employed to record the force signal, which will be the input data into a developed fuzzy broad learning system (FBLS). This FBLS system will return the surface roughness value of the workpiece.

2. Methodology

2.1 Measurement principle

The working principle of the proposed internal measurement method (hardware and software) is illustrated in Figure 1. In the hardware setup, the workpiece tube is mounted on a dynamometer which can measure the force exerted on the workpiece. A sphere magnet is placed inside the workpiece and an external magnet is used to drive the sphere magnet. The linear motion of the sphere magnet will produce a normal force (Fn) and a friction force (Ff) which will be recorded by the dynamometer. The force measured by the dynamometer is then sent to a fuzzy broad learning system (FBLS) [11] to generate the surface roughness data.

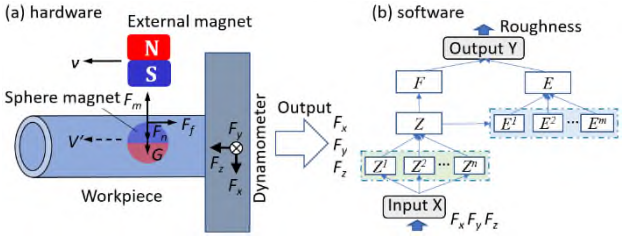

Figure 1. Working principle of the developed internal measurement technique: (a) schematic of the hardware and (b) the proposed FBLS

2.2 The developed fuzzy broad learning system (FBLS)

The basic architecture of FBLS is shown in Figure 1(b). Suppose that the FBLS consists of n fuzzy subsystems and m enhancement node groups, in which there are K_i fuzzy rules in the ith fuzzy subsystem, and there are L_j enhancement neurons in the jth enhancement node group. Given a training sample data set is represented as $S = \{X, Y\}$, $X = [x_1, x_2, \cdots, x_N]^T \in \mathbb{R}^{N\times M}$ and $Y = [y_1, y_2, \cdots, y_N]^T \in \mathbb{R}^{N\times 1}$ represent the input data and target output, respectively where $x_s = [x_{s1}, x_{s2}, \cdots, x_{sM}]$, $s = 1,2,\cdots,N$. N represents the number of training samples and M is the dimension of features for input data.

At first, the input $x_s = [x_{s1}, x_{s2}, \cdots, x_{sM}]$ is mapped to the ith fuzzy subsystem by using the first-order Takagi-Sugeno-Kang (TSK) fuzzy system. The fuzzy if-then rule in the i th fuzzy subsystem can be represented as:

if x_{s1} is A_k^i , x_{s2} is A_{k2}^i, …, and x_{sM} is A_{kM}^i, then one can get $z_{sk}^i = f_k^i(x_{s1}, x_{s2}, \cdots, x_{sM})$, where $k = 1,2,\cdots,K_i$.

The consequent part of the kth fuzzy rule can be defined by Eq. (1):

$$z_{sk}^i = \sum_{t=1}^{M} \alpha_{kt}^i x_{st} \tag{1}$$

where α_{kt}^i are randomly generated coefficients from a uniform distribution [0,1].

For the ith fuzzy subsystem, the fire strength of the kth fuzzy rule is given by Eq. (2):

$$\pi_{sk}^i = \prod_{t=1}^{M} \mu_{kt}^i(x_{st}) \tag{2}$$

where μ_{kt}^i is the Gaussian membership function corresponding to a fuzzy set A_{kt}^i, which is denoted by Eq. (3):

$$\mu_{kt}^i(x_{st}) = e^{-\left(\frac{x_{st}-c_{kt}^i}{\sigma_{kt}^i}\right)^2} \tag{3}$$

where c_{kt}^i and σ_{kt}^i represent the center and width of the Gaussian membership function, respectively. For the ith fuzzy subsystem, the K-means method on the training sample input data is used to obtain K_i clustering centers, which are used to initialize the centers c_{kt}^i of the Gaussian membership function. And for all fuzzy subsystems, the value of σ_{kt}^i is set to 1.

After that, the weighted fire strength of each fuzzy rule can be computed using Eq. (4):

$$\lambda_{sk}^i = \frac{\pi_{sk}^i}{\sum_{k=1}^{K_i} \pi_{sk}^i} \tag{4}$$

Before defuzzification by the TSK fuzzy subsystem, the intermediate output vector of the ith fuzzy subsystem for the sth training sample can be expressed by Eq. (5):

$$z_s^i = [\lambda_{s1}^i z_{s1}^i, \lambda_{s2}^i z_{s2}^i, \cdots, \lambda_{sK_i}^i z_{sK_i}^i] \tag{5}$$

And the intermediate output matrix of the ith fuzzy subsystem for all training samples can be denoted by Eq. (6):

$$Z^i = [z_1^i, z_2^i, \cdots, z_N^i]^T \tag{6}$$

Therefore, the intermediate output matrix for all fuzzy subsystems can be shown by Eq. (7):

$$Z = [Z^1, Z^2, \cdots, Z^n] \tag{7}$$

After that, the intermediate output matrix Z is fed into the enhancement nodes for nonlinear transformation. Then, the output matrix of the enhancement layer can be represented by Eq. (8):

$$E = [E^1, E^2, \cdots, E^m] \tag{8}$$

where $E^j = \psi(ZW_e^j + \beta_e^j)$, $j = 1,2,\cdots,m$. W_e^j and β_e^j are the weights and bias terms respectively, which are randomly generated from [0, 1] with proper dimensions. ψ is an activation function and is usually set as a hyperbolic tangent function ($tanh$).

Since the defuzzification output of each fuzzy subsystem and the output of the enhancement layer are transmitted to the top layer together, the defuzzification output of the i th fuzzy subsystem for the sth training sample can be expressed by Eq. (9):

$$F_s^i = \sum_{k=1}^{K_i} \lambda_{sk}^i z_{sk}^i = \sum_{k=1}^{K_i} \lambda_{sk}^i \left(\sum_{t=1}^{M} \omega_k^i \alpha_{kt}^i x_{st}\right) = \sum_{t=1}^{M} \alpha_{kt}^i x_{st} [\lambda_{s1}^i, \lambda_{s2}^i, \cdots, \lambda_{sK_i}^i] \begin{bmatrix} \omega_1^i \\ \omega_2^i \\ \vdots \\ \omega_{K_i}^i \end{bmatrix} \tag{9}$$

where the parameter ω_k^i is introduced to adjust the kth fuzzy rule, and can be defined by Eq. (10):

$$\omega^i = [\omega_1^i, \omega_2^i, \cdots, \omega_{K_i}^i]^T \tag{10}$$

The above formula can be simplified to Eq. (11):

$$F_s^i = z_s^i \omega^i \tag{11}$$

For all training samples, the defuzzification output of the ith fuzzy subsystem is Eq. (12):

$$F^i = [F_1^i, F_2^i, \cdots, F_N^i]^T = Z^i \omega^i \tag{12}$$

Then, the defuzzification output of all fuzzy subsystems can be aggregated by Eq. (13):

$$F = \sum_{i=1}^{n} F^i = ZW_F \tag{13}$$

where $W_F = [\omega^1, \omega^2, \cdots, \omega^n]^T$.

In the end, the defuzzification output F of all fuzzy subsystems and the output E of enhancement node groups will be concatenated into a matrix to obtain the final output of FBLS, which can be expressed by Eq. (14):

$$\hat{Y} = F + EW_E = ZW_F + EW_E = [Z \quad E] \begin{bmatrix} W_F \\ W_E \end{bmatrix} \tag{14}$$

where W_E denotes the weight matrix from the enhancement layer to the top layer.

Let $H = [Z, E]$, $W = [ZW_F, W_E]^T$, Then $\hat{Y}$ can be abbreviated by Eq. (15):

$$\hat{Y} = HW \tag{15}$$

Given the actual training target Y, the weight matrix W from the hidden layer to the final output layer can be calculated by ridge regression using Eq. (16):

$$W = (H^T H + \lambda I)^{-1} H^T Y \tag{16}$$

in which I denotes an identity matrix with proper dimensions and λ is a nonnegative constant for regularization.

3. Experiments and validation

3.1 Experimental setup

A measurement setup (Figure 2) is built based on the schematic in Figure 1(a). An external magnet is fixed on the moving axis of a three-axis automatic stage (Sherline Products Inc). The workpiece is an Al6061 plate with milled grooves to simulate the internal surface of a tube. It is mounted on a fixture connecting a dynamometer (Kistler 9256C). A sphere magnet with an 8-mm diameter is placed on the groove. Due to the magnetic force, the sphere magnet can be driven to slide on the groove surface while the dynamometer records the force interactions simultaneously. It should be noted that the dynamometer may be replaced by cheaper and portable sensors (e.g., acceleration/vibration sensors) in practical applications.

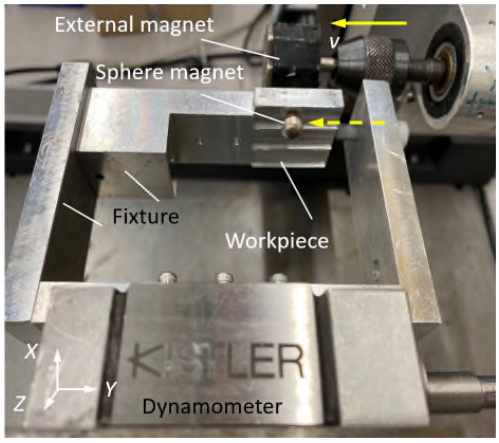

Figure 2. Experimental setup for data acquisition

3.2 Workpiece preparation and data acquisition

Totally 8 workpieces are prepared by end milling at a Makino V55 vertical milling machine. Three grooves are cut in each workpiece and a total of 23 grooves are machined (one groove failed due to tool breakage). The milling parameters i.e., spindle speed, feed rate, and tool wear condition, are varied to generate grooves with a large range of surface finish. Specifically, the varying of tool wear conditions is achieved by using milling tools with different VB values. After milling, the groove surfaces are scanned by a laser confocal microscope (Olympus LEXT OLS5000) and the surface roughness Ra is measured with a cut-off length of 0.25 mm. Three measurements are conducted for each groove. The resultant surface roughness ranges from 0.193 µm to 9.787 µm, covering the typical finish of engineering surfaces [12].

To acquire the force signal for the developed FBLS, the sphere magnet is driven to slide on the groove for 20 mm with a feed rate of 100 mm/min. And the corresponding force is recorded by the dynameter with a sampling frequency of 50 kHz. The parameters of the data acquisition process are listed in Table 1.

Table 1. Parameters of the data acquisition process for surface roughness measurement

Parameters	Values
External magnet	NdB G50 block magnet 20 mm × 10 mm × 6 mm
Sphere magnet	NdB G35 sphere magnet with 8 mm diameter
Workpiece	A6061 Aluminium plate, 8 pcs, and 23 grooves
The gap distance (mm)	5
Scratching distance (mm)	20
Feed rate (mm/min)	100
Sampling rate (kHz)	50

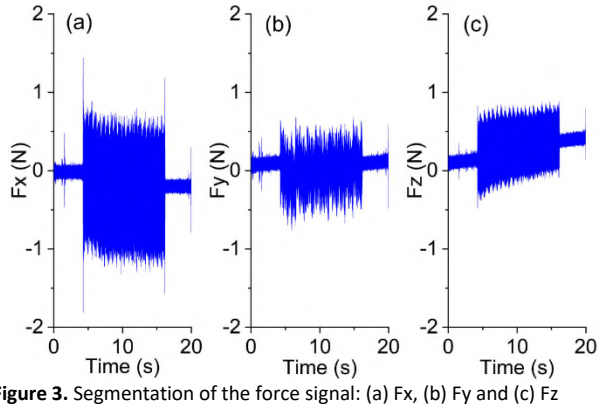

Figure 3. Segmentation of the force signal: (a) Fx, (b) Fy and (c) Fz

3.3 Pre-process of the collected force data

The X, Y, and Z force signals are effectively segmented by removing the near-zero sections at the beginning and the end, as shown in Figure 3. Besides, 8 representative time-domain features are extracted from the force signals in the three directions of X, Y, and Z, respectively, as the input of the model, with a total of 24 features, as shown in Table 2.

Table 2. Time-domain features of the force signals

No.	Feature	Equation
1	Absolute average	$X_u = \frac{1}{n}\sum_{i=1}^{n}\lvert x_i\rvert$
2	Variance	$X_{var} = \frac{1}{n}\sum_{i=1}^{n}(x_i - \bar{x})^2$
3	Standard deviation	$X_{std} = \sqrt{Xvar}$
4	Peak-to-Peak value	$X_{pv} = max(x_i) - min(x_i)$
5	Kurtosis	$X_{kur} = \frac{\sum_{i=1}^{n}(x_i-\bar{x})^4/n}{\left[\sum_{i=1}^{n}(x_i-\bar{x})^2/n\right]^2}$
6	Skewness	$X_{ske} = \frac{\sum_{i=1}^{n}(x_i-\bar{x})^3/n}{\left[\sum_{i=1}^{n}(x_i-\bar{x})^2/n\right]^{3/2}}$
7	Root mean square	$X_{rms} = \sqrt{\frac{1}{n}\sum_{i=1}^{n} x_i{}^2}$
8	Shape factor	$X_{sf} = \frac{X_{rms}}{X_u}$

4. Results

In this case study, a total of 23 groups of the force data set were collected, of which 16 data set were randomly selected for model training, and the remaining 7 samples were used for model testing.

As seen in Table 2, the time-domain features have different dimensions and unit magnitudes. Thus, it is necessary to normalize the data using a standardized transformation method. Herein the min-max standardization approach is adopted, as expressed in Eq. (17):

$$\bar{x_i} = \frac{x_i - x_{min}}{x_{max} - x_{min}} \tag{17}$$

where x_{max} and x_{min} represent the maximum and minimum values of feature x, respectively.

To verify the feasibility of the model in predicting the surface roughness, the root-mean-square error (RMSE), mean absolute error (MAE), and mean absolute percentage error (MAPE) can be selected as the evaluation performance indicators respectively, which are expressed in Eqs. (18–20):

$$RMSE = \sqrt{\frac{1}{n}\sum_{i=1}^{n}(y_i - \hat{y_i})^2} \tag{18}$$

$$MAE = \frac{1}{n}\sum_{i=1}^{n}\lvert y_i - \hat{y_i}\rvert \tag{19}$$

$$MAPE = \frac{1}{n}\sum_{i=1}^{n}\left\lvert\frac{y_i - \hat{y_i}}{y_i}\right\rvert \times 100\% \tag{20}$$

in which n is the number of observations, y_i and y_i represent the actual and predicted values for sample i, respectively.

Figure 4 presents the prediction results of the surface roughness (Ra) of the grooves by FBLS, and the values of the predictive errors are listed in Table 3. The predicted Ra shows good agreement with the experimental Ra for all evaluation criteria. Particularly, the model shows good predicting accuracy when the surface roughness Ra is larger than 1 µm if the RMSE and the MAE are employed as the evaluation criteria (Actually, there is no difference by using RMSE and MAE as the evaluation criteria), as shown in Figure 4(a) and (b). On the other hand, the model using MAPE can provide accurate predictions for the whole range of different surface finish except the Testing No. 6 (Ra 3.163 µm), as seen in Figure 4(c). Figure 5 shows the variation of RMSE against the numbers of fuzzy subsystems and fuzzy rules. With the increase in the number of fuzzy subsystems and fuzzy rules, the RMSE tends to decrease. Particularly, the influence of fuzzy rules on the RMSE is more significant. In a

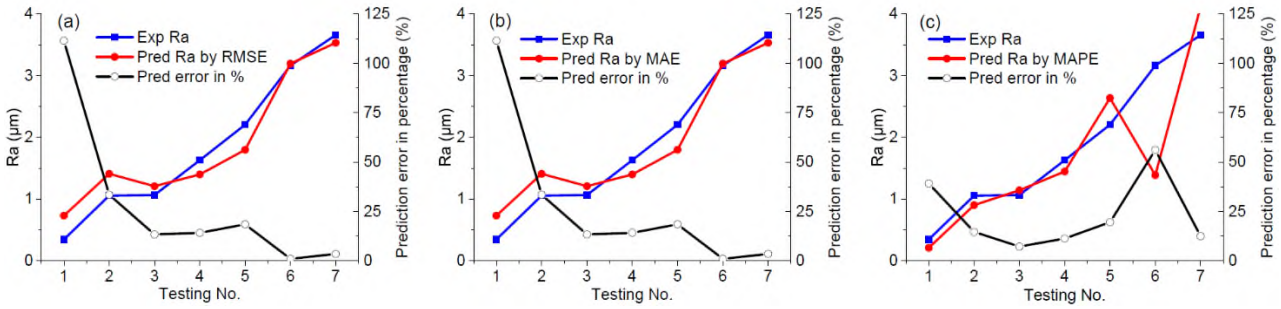

Figure 4. Measured and predicted surface roughness Ra under different evaluation criteria: (a) RMSE, (b) MAE and (c) MAPE.

word, the investigations demonstrate that the proposed method is easy to implement and can yield a promising predicting outcome compared with the X-ray CT method [9] and the AE method [10]. The proposed method also exhibits great potential to measure the surface roughness of complex internal surfaces.

Table 3. Measured surface roughness Ra and the predictive errors under different evaluation criteria i.e., RMSE, MAE and MAPE, respectively

Testing No.	Measured Ra (μm)	By RMSE (%)	By MAE (%)	By MAPE (%)
1	0.346	111.4	111.4	39.1
2	1.056	33.4	33.4	14.6
3	1.066	13.4	13.4	7.2
4	1.630	14.2	14.2	11.2
5	2.206	18.5	18.5	19.6
6	3.163	1.0	1.0	56.1
7	3.659	3.5	3.5	12.4

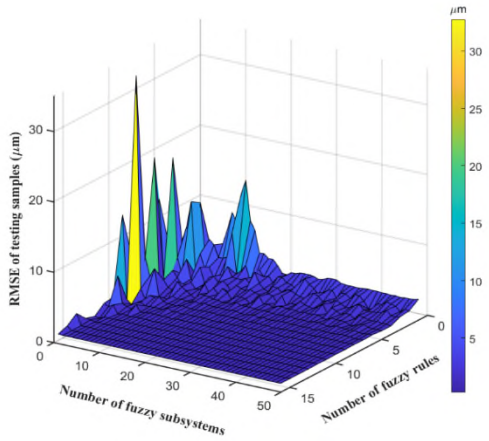

Figure 5. Dependence of RMSE values against the number of fuzzy subsystems and the number of fuzy rules

5. Conclusion Remarks

Leveraging the advantages of machine learning, this paper proposed novel internal surface measurement methods via a magnetic ball scratching on the workpiece surface. A measuring setup was built and Alumiunium workpieces with milled grooves were employed as the specimens. The force interaction between the magnetic ball and the workpiece was obtained and pre-processed before being fed into a proposed fuzzy broad learning system (FBLS). By training the FBLS with limited data sets, this model demonstrates an average measurement error (using the measured Ra by a stylus profilometer as a reference) of only 10.1% for the surfaces with a roughness larger than 1 μm Ra, though the errors for finer surfaces are inadequate. The results indicate that the current measuring technique may be helpful to additively manufactured raw components that exhibt a relative rough surfaces. Future work will focus on integrating other signals (acceleration/vibration which uses much cheaper and more portable sensors rather than the dynamometer) as the input and exploring other machine learning models to improve the measuring accuracy of fine surfaces.

Acknowlegement

This research is supervised by Dr Hao Wang of the Department of Mechanical Engineering, National University of Singapore (email: mpewhao@nus.edu.sg) and financially supported by the Singapore Ministry of Education Academic Research Funds (Grant Nos.: A-8001225-00-00, MOE-T2EP50120–0010 and MOE-T2EP50220–0010). The proposed method has been filed as a PCT application (PCT/SG2023/050771).

References

[1] J. Zhang, W. Tian, F. Zhao, X. Mei, G. Chen, H. Wang, Material Removal Rate Prediction Based on Broad Echo State Learning System for Magnetically Driven Internal Finishing, *IEEE Trans. Ind. Informatics*. (2022). https://doi.org/10.1109/TII.2022.3204003.

[2] M. Kumar, M. Das, N. Yu, Surface Roughness Simulation During Rotational–Magnetorheological Finishing of Poppet Valve Profiles, *Nanomanufacturing Metrol*. **5** (2022) 259–273.

[3] J. O'Hara, F. Fang, Magnetohydrodynamic-based Internal Cooling System for a Ceramic Cutting Tool: Concept Design, Numerical Study, and Experimental Evalidation, *Nanomanufacturing Metrol.* **6** (2023) 33. https://doi.org/10.1007/s41871-023-00210-9.

[4] J. Zhang, H. Wang, Magnetically driven internal finishing of AISI 316L stainless steel tubes generated by laser powder bed fusion, *J. Manuf. Process.* **76** (2022) 155–166. https://doi.org/10.1016/j.jmapro.2022.02.009.

[5] Z. Liu, Q. Guo, Y. Sun, W. Wang, W. Zhao, Z. Yang, Surface roughness and burr generation in micro-milling: A review, *J. Adv. Manuf. Sci. Technol.* **4** (2024) 2023017–0. https://doi.org/10.51393/j.jamst.2023017.

[6] M.W. Lindner, White-light interferometry via an endoscope, in: Interferom. *XI Tech. Anal.*, SPIE, 2002: pp. 90–101.

[7] J. Zhang, H. Wang, Generic model of time-variant tool influence function and dwell-time algorithm for deterministic polishing, *Int. J. Mech. Sci.* **211** (2021) 106795. https://doi.org/10.1016/j.ijmecsci.2021.106795.

[8] J.P. Kruth, M. Bartscher, S. Carmignato, R. Schmitt, L. De Chiffre, A. Weckenmann, Computed tomography for dimensional metrology, *CIRP Ann. - Manuf. Technol.* **60** (2011) 821–842. https://doi.org/10.1016/j.cirp.2011.05.006.

[9] A. Du Plessis, I. Yadroitsev, I. Yadroitsava, S.G. Le Roux, X-Ray Microcomputed Tomography in Additive Manufacturing: A Review of the Current Technology and Applications, *3D Print. Addit. Manuf.* **5** (2018) 227–247. https://doi.org/10.1089/3dp.2018.0060.

[10] Z.M. Hafizi, C.K.E. Nizwan, M.F.A. Reza, M.A.A. Johari, High Frequency Acoustic Signal Analysis for Internal Surface Pipe Roughness Classification, in: *Appl. Mech. Mater., Trans Tech Publ*, 2011: pp. 249–254.

[11] S. Feng, C.L.P. Chen, Fuzzy broad learning system: A novel neuro-fuzzy model for regression and classification, *IEEE Trans. Cybern.* **50** (2018) 414–424.

[12] J.T. Black, R.A. Kohser, DeGarmo's Materials and Processes in Manufacturing, Eleventh, *John Wiley & Sons, Inc.*, 2011.